

Supplementary material

Tao Sun^{a,b}, Zhendong Dai^a, Poramate Manoonpong^{a,b,*}

^a*Institute of Bio-inspired Structure and Surface Engineering, College of Mechanical and Electrical Engineering, Nanjing University of Aeronautics and Astronautics, Nanjing, China*

^b*Embodied AI & Neurorobotics Lab, SDU Biorobotics, the Mærsk Mc-Kinney Møller Institute, the University of Southern Denmark, Odense M, Denmark*

1. Dynamical movement primitives (DMPs)-based control with DFRL

Dynamical movement primitives (DMPs) are an effective approach towards constructing the desired oscillators for rhythmic movement control [1, 2]. DMPs can imitate the outputs of any type of central pattern generator (CPG) efficiently via an optimization technique (e.g., locally weighted regression (LWR)) [3]. In this supplementary material, we integrate the DMPs-based control with the DFRL. Here, the DMPs serve as CPGs, generating periodic commands for driving the joint movements of a quadruped robot. The DFRL is directly integrated with the DMPs-based control, to adapt the offsets of the DMP outputs. As shown in Fig. S.1, under the DMPs-based control, the DMPs act as CPGs instead of the SO(2) oscillators. The DMPs consist of four DMP units, each DMP unit (featuring two DMP oscillators) is responsible for the two joint movement controls of a leg. The DMP oscillator model can be described as [2, 4]

$$\begin{aligned} \tau \dot{z} &= \alpha_z (\beta_z (g - y) - z) \\ \tau \dot{y} &= z + f \end{aligned}, \quad (\text{S.1})$$

where α_z and β_z are time constants, and g is a set point of the trajectory, which acts as the baseline of the oscillation. f is a nonlinear function approximator; it uses local linear models of basis functions, as

$$\begin{aligned} f &= \frac{\sum_{k=1}^N \Psi_k \mathbf{w}_k^T}{\sum_{i=1}^N \Psi_i}, \\ \Psi_k &= e^{(h_k (\cos(x - c_k) - 1))}, \\ \tau \dot{x} &= 1, \end{aligned} \quad (\text{S.2})$$

where \mathbf{w}_k is the parameter vector of the k -th local model; it is determined by LWR learning [3] from a demonstrated trajectory generated by the SO(2)-based CPG. h_k and c_k determine the width and center of the basis functions, respectively. N is the number of basis functions. The parameter values in the following investigations can be seen in Table S.1

Table S.1: Parameter values of the DMPs.

Parameters	τ	α_z	β_z	g	y_0	dt	N
Values	6	25	6.25	0	0	0.01	200

The data used for training the DMP unit are taken from the two outputs of the SO(2)-based CPG (see Fig. S.2). Using the LWR, the DMP unit can output two signals (o_1 and o_2), similar to the two outputs of the SO(2)-based CPG (Fig. S.4).

*Corresponding author

Email addresses: s.tao@nuaa.edu.cn (Tao Sun), zddai@nuaa.edu.cn (Zhendong Dai), poma@nuaa.edu.cn (Poramate Manoonpong)

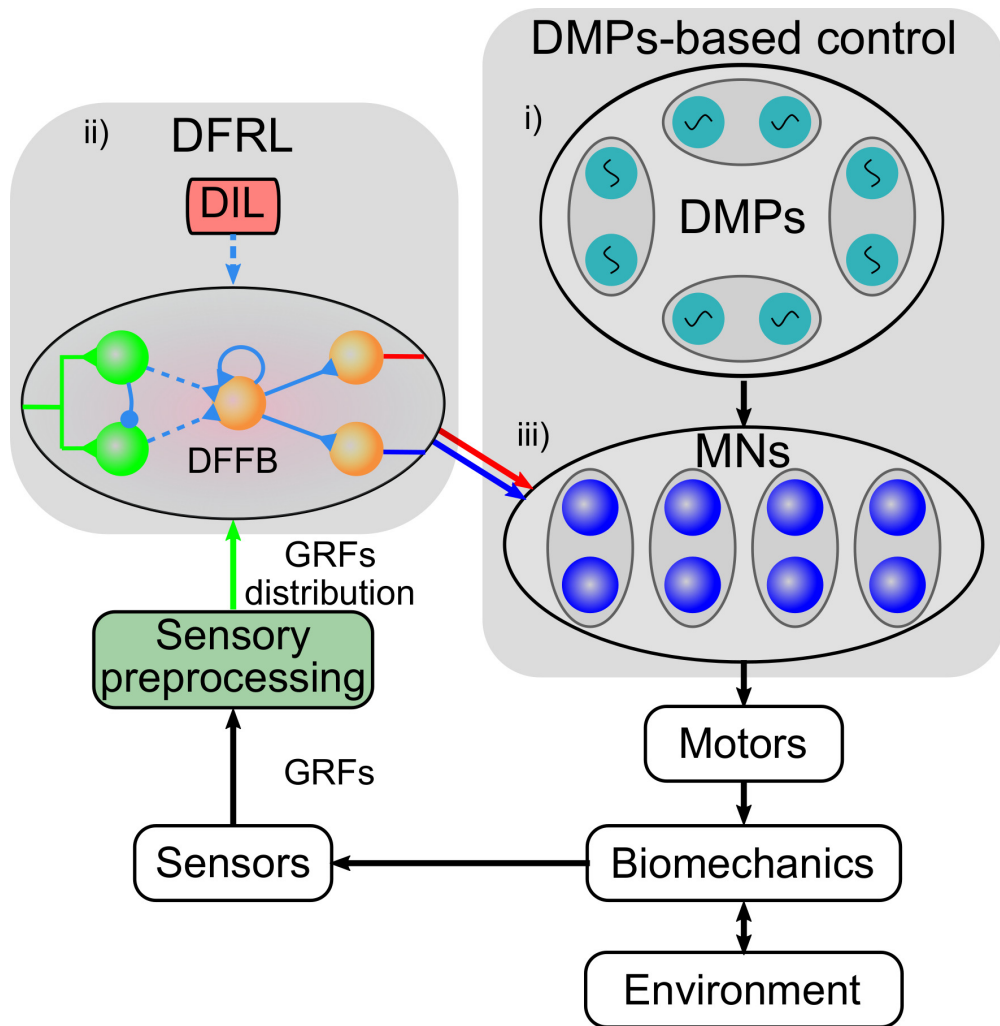


Figure S.1: Schematic diagram of the DMPs-based control integrated with the DFRL. It features (i) four DMP units for generating multi-dimensional rhythmic commands; (ii) the DFRL (including the DFFB reflex and DIL), using GRF information for the DMP output offset adaptation; and (iii) the MNs for integrating and transferring adaptive commands from the DMPs and DFFB reflex to control robot leg-joint movements.

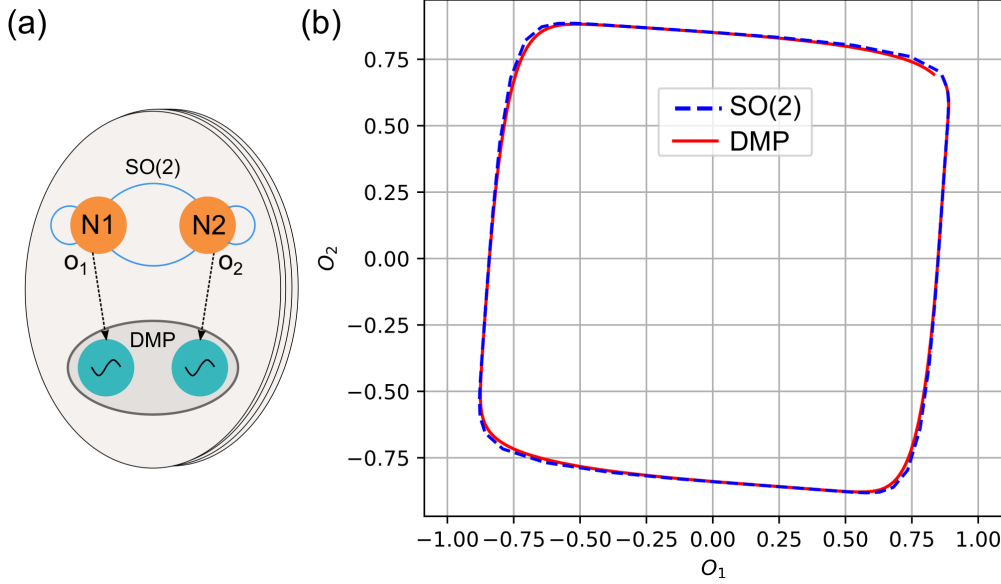


Figure S.2: DMP unit training using the SO(2)-based CPG outputs. (a) The SO(2)-based CPG outputs serve as desired trajectories with which to train a DMP unit using LWR. (b) The SO(2)-based CPG and DMP unit outputs in a phase diagram.

2. Implementation of the DMPs-based DFRL control in a quadruped robot

To evaluate the performance of the integrated DMPs and DFRL, we implemented the DMPs-based DFRL control in Lilibot, and we tested the robot for different initial joint offsets on level ground (see Fig. 9 in the main manuscript). This experiment is comparable to Experiment I for the CPG-based control, shown in the main manuscript (see Fig. 10)

Fig. S.3 shows the real-time data for a trial in the extreme C_7 condition as an example. Lilibot can be seen to quickly form a regular trot gait and stably move forward after interacting with the ground (i.e., within 3 s). In addition, the robot body oscillation decreases significantly. The convergence progress in all seven conditions can be seen in Fig. S.4. The plastic weights ($w_{1,2}$) of the DFRL are adaptable, which affects the changes of the joint offsets ($\beta_{1,2}$). The joint offsets are online-adjusted by the DFFB reflex of the DFRL. As a result, the joint offsets for one leg (e.g., right-front leg) quickly converge to particular values under all conditions and from different initializations. With the joint offsets stabilized, the plastic weights converge to certain values, producing DFFB reflex gains. In addition, the smoothed GRF distribution parameter ($\bar{\gamma}$) also converges to a constant value of approximately 1.1. After the offsets become stable, the roll and pitch angles of the robot posture are reduced.

The experimental results demonstrate that the DFRL can also implement DMPs-based control to generate proper motor commands (with offset adaptation) and thereby obtain appropriate body postures and stable locomotion. This suggests that the DFRL design is generic and independent of specific CPGs. The DFRL can be directly integrated into different CPGs, such as DMP and SO(2).

3. Stability analysis of quadruped robot trotting on slopes using a simplified model

3.1. Modeling

Intuitively ensuring stable trotting behavior in a quadrupedal robot on slope terrains is a complicated task; it involves several factors (e.g., control, structure, material, power, friction, etc.) that must meet certain specific conditions, as described in the discussion section. In this paper, we focus on body posture stability for stable locomotion. Fig. S.5 illustrates a simplified model for analyzing the body-posture stability conditions of a quadruped robot trotting upon a slope. In this analytical model, we assume the following:

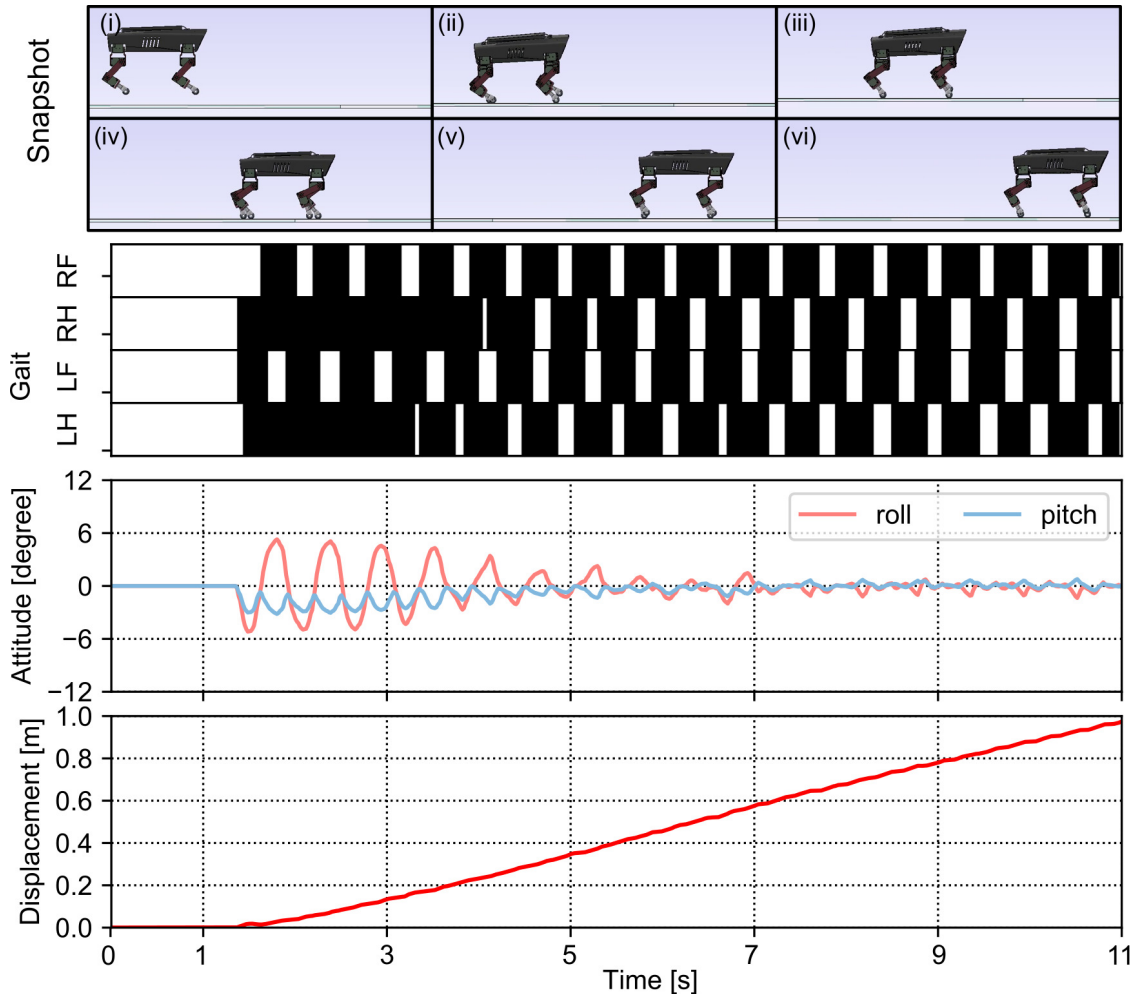


Figure S.3: Real-time data for a C_7 condition trial, using the DMPs-based DFRL control. A stable trot gait with few body oscillations emerged after ~ 5 s. The black region in the gait diagram indicates the stance phase, whilst the white region indicates the swing phase of each leg (RF: right-front leg, RH: right-hind, LF: left-front, LH: left-hind).

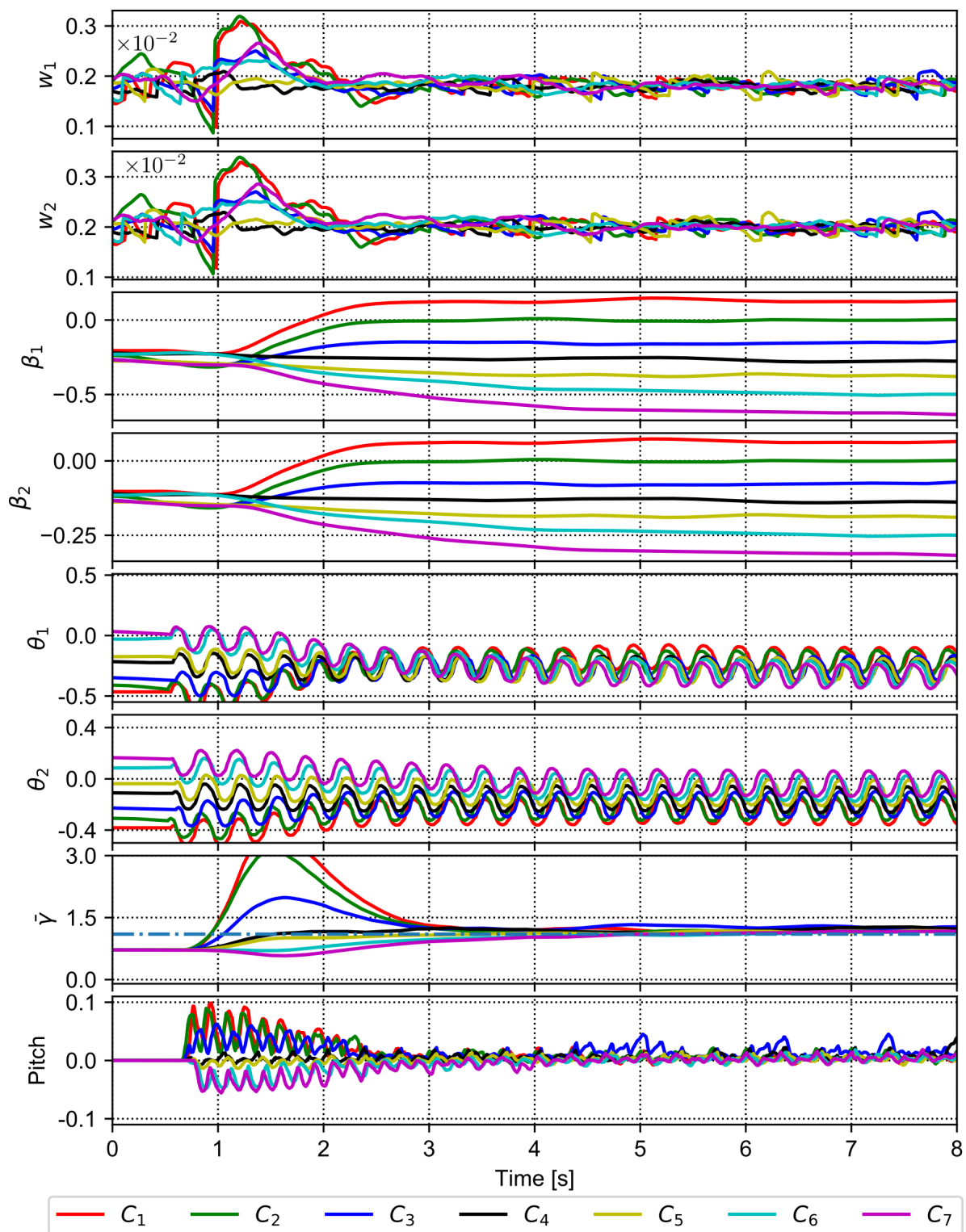


Figure S.4: Real-time data for all conditions in Experiment I (walking on level ground) using the DMPs-based DFRL control. w_1 and w_2 are the plastic weights of the DFFB reflex network (see Fig. 5 in the main manuscript); they are online-adjusted by the DIL (see Eqs. (11) and (12)). β_1 and β_2 are the hip and knee joint command offsets for a leg (i.e., the right-front leg), and they are automatically adjusted by the DFFB reflex (see Eq. (10)). The hip and knee joint commands for the leg are θ_1 and θ_2 , respectively. Their offsets converge to constant values within ~ 5 s. $\bar{\gamma}$ converged to ~ 1.1 . The pitch angle of the robot body, with respect to body stability, becomes notably smaller after offset convergence.

(1) the leg mass is negligible and the center of mass is located in the center of the body, because most of the robot's mass is located in its base; (2) Coriolis and centrifugal forces are negligible (this is reasonable here because the robot moves slowly); (3) the feet do not slip on the surface (feet are enacted with sufficient frictional force) and cannot generate moments at the contact because the feet have an almost point-like contact area [5]. Based on these assumptions, an equilibrium constraint of the stability conditions, which satisfies both front and hind stance feet lifting criteria, can be described as follows:

$$F_h \cdot x_1 = F_f \cdot x_2. \quad (\text{S.3})$$

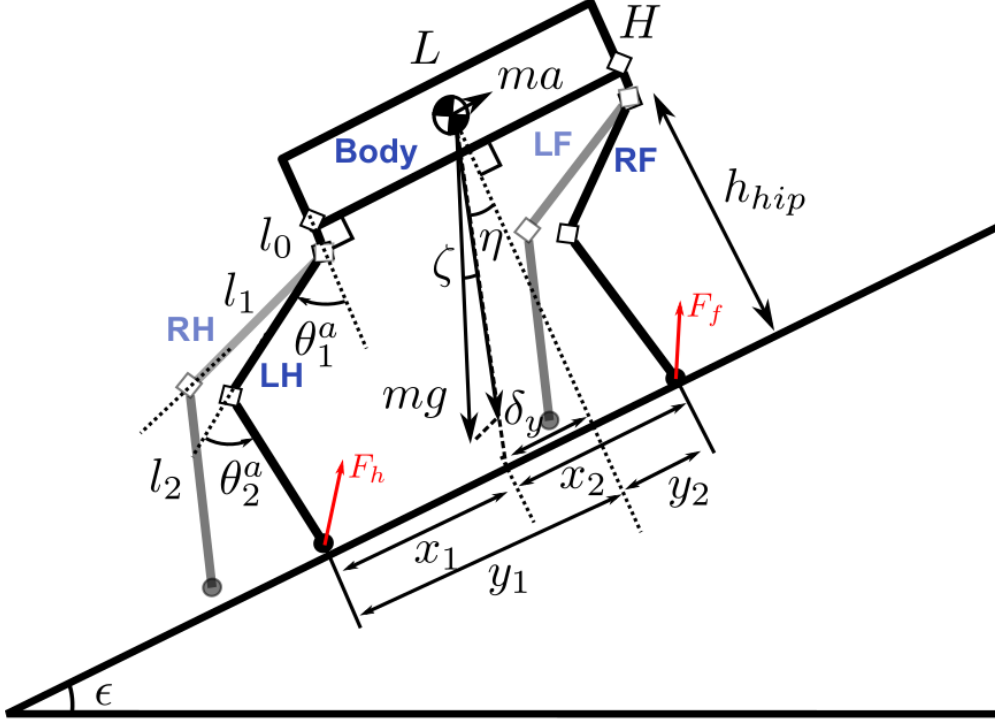


Figure S.5: Simplified model of a quadruped robot trotting on a slope in the sagittal plane. The robot is modeled as a rigid body connected to four identical legs, each of which consists of three connected massless links: l_0 , l_1 , and l_2 . The mass of the body m is located at its base, and the dimensions of the body are referred to as $L \cdot H$. ma and mg represent the inertial force and gravity acting upon the body, respectively. $\theta_{1,2}^a$ are the anterior extreme positions of the hip and knee joints, respectively. F_f and F_h represent the front and hind GRFs, respectively. ϵ represents the slope inclination.

From the geometric relationship of the model in Fig. S.5, we obtain the following equations:

$$\begin{aligned} x_1 &= y_1 - \delta_y, \\ x_2 &= y_2 + \delta_y. \end{aligned} \quad (\text{S.4})$$

Using the leg's forward kinematics, the variables in Eq. (S.4) can be expressed as

$$\begin{aligned} \delta_y &= (H/2 + l_0 + h_{hip}) * \tan(\eta), \\ y_1 &= L/2 + l_1 * \sin(\theta_1^a) - l_2 * \sin(\theta_2^a - \theta_1^a), \\ y_2 &= L/2 - l_1 * \sin(\theta_1^a) + l_2 * \sin(\theta_2^a - \theta_1^a), \end{aligned} \quad (\text{S.5})$$

where L and H are the length and height of the robot body, $l_{0,1,2}$ are the lengths of the leg links, and h_{hip} is the height from the hip to the surface. $\theta_{1,2}^a$ are the extreme anterior positions of the hip and knee joints, respectively; these can be determined by the joint command offsets.

From the geometric restrictions, we obtain the h_{hip} and η of Eq. (S.5) as

$$\begin{aligned} h_{hip} &= l_1 * \cos(\theta_1^a) + l_2 * \cos(\theta_2^a - \theta_1^a), \\ \eta &= \epsilon - \zeta, \end{aligned} \quad (\text{S.6})$$

where ϵ denotes the slope inclination.

By combining Eqs. (S.3), (S.4), (S.5), and (S.6), we obtain the relationship between the joint anterior extreme positions ($\theta_{1,2}^a$) and slope inclinations (ϵ) upon which the robot can steadily trot without considering other conditions (e.g., joint torque limit, feet friction force, uneven surface, etc.); this relationship is expressed as

$$\epsilon = \arctan\left(\frac{l_1 * \sin(\theta_1^a) - l_2 * \sin(\theta_2^a - \theta_1^a)}{H/2 + l_0 + l_1 * \cos(\theta_1^a) + l_2 * \cos(\theta_2^a - \theta_1^a)}\right) + \zeta. \quad (\text{S.7})$$

Assume that $\Delta\theta_{1,2}$ represents the joint movement ranges of the hip and knee joints, respectively; then, we can obtain the joint command offsets as follows:

$$\beta_{1,2} = \theta_{1,2}^a - \Delta\theta_{1,2}/2. \quad (\text{S.8})$$

Eqs. (S.7) and (S.8) express the relationship between the joint command offsets ($\beta_{1,2}$) and conquerable slopes (ϵ). Although this derivation neglects certain realistic restrictions, it explains how the proper joint-command offsets stabilize the robots trot behavior on slopes; furthermore, it provides a quantitative guideline for modulating the trot-stabilizing offsets. Thus, it predicts the maximum slope inclination upon which a quadruped robot can trot, in terms of its leg and body dimensions and joint movement ranges ($l_0, l_1, l_2, H, \Delta\theta_{1,2}$).

3.2. Maximum slope inclinations upon which Lilibot and Laikago can trot

Based on the foregoing conclusion, we can calculate the maximum slope inclination that Lilibot can traverse. The configuration of Lilibot is shown in Table S.2. Substituting these parameters into Eq. (S.7), we obtain a visualization of the conquerable slopes, as shown in Fig. S.6. The graph reveals that the maximum slope inclination (ϵ_{max}) upon which Lilibot can trot is $\sim 35.6^\circ$ when $\theta_1^a = 80^\circ$ and $\theta_2^a = 50^\circ$; meanwhile, the minimum slope (ϵ_{min}) is $\sim -36.2^\circ$ when $\theta_1^a = 0^\circ$, $\theta_2^a = 110^\circ$. For Laikago, $\epsilon_{max} = 50^\circ$ when $\theta_1^a = 85^\circ$ and $\theta_2^a = 50^\circ$; meanwhile, $\epsilon_{min} = -45.8^\circ$ when $\theta_1^a = 0^\circ$ and $\theta_2^a = 110^\circ$. These results are based on three assumptions: the feet can obtain sufficient frictional force, the joint motor can provide sufficient power, and the inertial force (ma) can be neglected because the locomotion speed is relatively slow.

4. Postural modulation strategies for slope locomotion

A quadrupedal robot trotting on a slope requires additional body posture modulation to maintain stability. Two postural modulation strategies are possible: telescoping strut and lever mechanics (see Fig. S.7).

Without a postural modulation strategy (see Fig. S.7 (a)), gravity places a large load on the hind legs of the robot during uphill locomotion; thus, x_1 is significantly smaller than x_2 , and γ is subsequently below its standard value. Consequently, the hind legs are unable to lift. Conversely, implementing postural modulation alongside either of these two strategies ensures an appropriate GRF distribution or γ for stably lifting the feet; however, this modulation operates differently under the two strategies.

¹ $\theta_{1,2}^a$ are determined by the joint structure configuration. ζ can be approximately set to zero when the robot has a relatively low walking speed.

Table S.2: The main specifications of Lilibot and Laikago.

Parameters ¹	Values	
	Lilibot	Laikago
m	2.5 Kg	25 Kg
H	0.07 m	0.15 m
L	0.32 m	0.55 m
l_0	0.04 m	0.08 m
l_1	0.07 m	0.41 m
l_2	0.086 m	0.45 m
θ_1^a	0° - 80°	0° - 85°
θ_2^a	50° - 110°	50° - 110°
ζ	0°	0°
Total DOFs	12	12
Force sensors	4	4

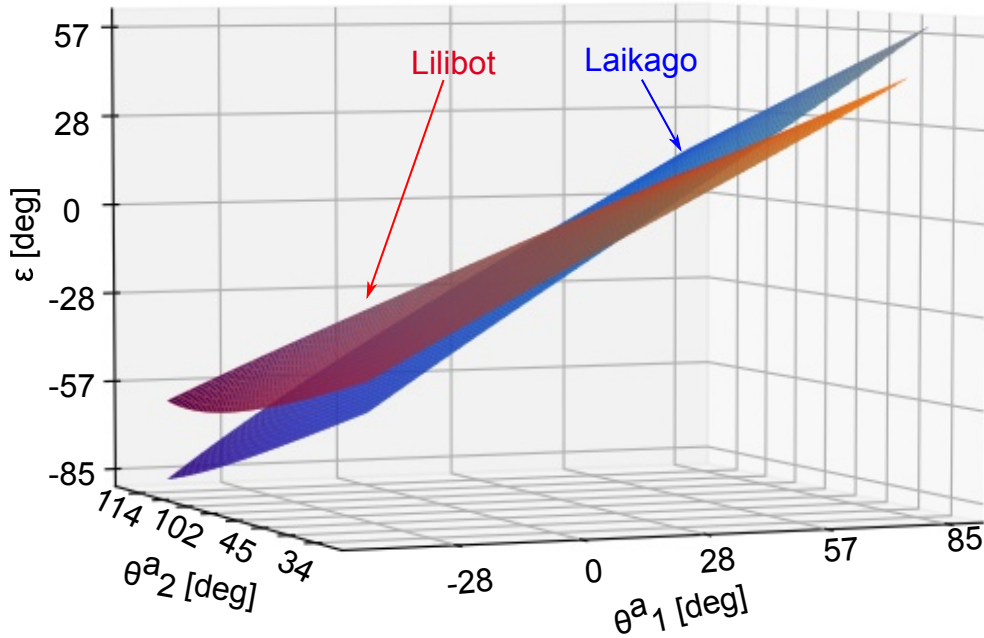


Figure S.6: Visualization of the relationship between the joint anterior extreme positions and the conquerable slope inclinations of Lilibot and Laikago.

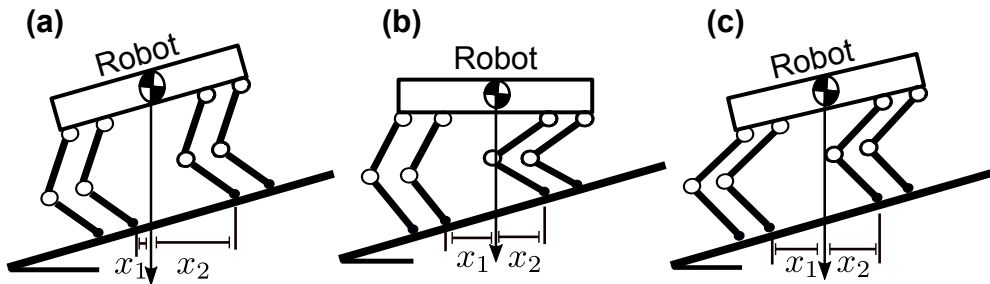


Figure S.7: Postural modulation strategies for quadruped robots trotting on slopes. (a), (b), and (c) denote the strategies of no postural modulation, telescoping strut, and lever mechanics, respectively.

5. Vestibular reflex mechanism

The vestibular reflex mechanism is shown in Fig. S.8. The reflex inputs body posture angles (i.e., pitch and roll) as sensory feedback to generate responses. The outputs of the reflex are transferred to the MNs to adjust the CPG/joint offsets. As a result, the joint movements are adjusted to realize a certain body posture.

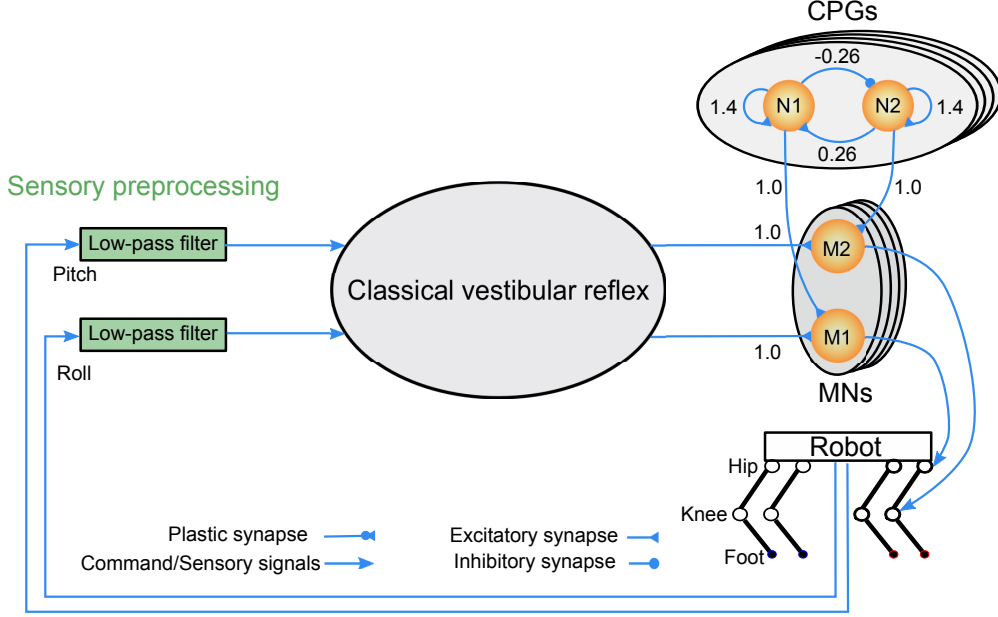


Figure S.8: Diagram of CPG-based control using the vestibular reflex. The reflex adjusts the robots posture using the telescoping strut strategy [6].

6. Performance metrics

6.1. Stability

Large-amplitude changes in body orientation (i.e., roll and pitch) are known to decrease locomotion stability; that is, they negatively affect the conservation of momentum and increase the risk of the robot falling [7, 8]. The pitch angle is influenced by the slopes upon which the robot is trotting. Therefore, only the maximum standard deviation of the body roll angle is used to represent its stability during locomotion. The detailed definition is

$$r\bar{oll} = \frac{1}{N} \sum_{n=0}^N roll(n), \quad (S.9)$$

$$roll_{std} = \sqrt{\frac{1}{N-1} \sum_{n=0}^N (roll(n) - r\bar{oll}(n))^2}, \quad (S.10)$$

where N is the total sample size of the body roll angle $roll(n)$. Eqs. (S.9) and (S.10) produce the mean and standard deviation of the roll angle during locomotion, respectively.

The standard deviation of the roll angle indicates the amplitude of oscillations within a period. Its inverse is defined as a stability metric, as shown in Eq. (S.11). Thus, the larger the *stability* value, the more stable the locomotion.

$$stability = \frac{1}{roll_{std}}. \quad (\text{S.11})$$

6.2. Coordination

In addition to the body movement state, the robots foot motions also significantly determine locomotive performance. Here, we implement a symmetrical robot control in which each identical leg derives its control commands from only the phase shift under a trot gait. Ideally, all robot feet should then be able to perform similar alternating movements from swing to stance. Thus, all legs should have the same duty factors during stable trotting. The coordination metric is used to measure the consistency of duty factors; it is defined as

$$\mu_i(m) = \frac{T_{swing}^i(m)}{T_{swing}^i(m) + T_{stance}^i(m)}, \quad (\text{S.12})$$

$$\bar{\mu}(m) = \frac{1}{4} \sum_{i=1}^4 (\mu_i(m)), \quad (\text{S.13})$$

$$\mu_{std}(m) = \begin{cases} \sqrt{\frac{\sum_{i=1}^4 (\mu_i(m) - \bar{\mu}(m))^2}{3}} & \forall m \leq M, i \leq 4, \exists \mu_i(m) \\ 0 & \text{otherwise} \end{cases}, \quad (\text{S.14})$$

$$coordination = \begin{cases} \frac{1}{\max_{\{m \in M\}} (\mu_{std}(m))} & \exists \mu_{std}(m) \neq 0 \\ 0 & \text{otherwise} \end{cases}, \quad (\text{S.15})$$

where $T_{swing}^i(m)$ and $T_{stance}^i(m)$ in Eq. (S.12) denote the swing and stance periods of the i -th leg during the m -th step, respectively. Thus, $\mu_i(m)$ defines the duty factor of the m -th step for the i -th leg, and the mean ($\bar{\mu}(m)$) and standard deviation ($\mu_{std}(m)$) of the duty factor for the four legs (at the m -th step) are output to measure the irregularity/incongruity of the four leg movements. The inverse of the maximum standard deviation over several steps (i.e., M) was used to characterize the coordinated movements of the four legs. Therefore, the larger the *coordination* value, the greater the coordination of a regular trot gait.

6.3. Displacement

Displacement is a basic measure of legged robot locomotion. Thus, we invoke a *displacement* metric. It is defined as the locomotive displacement of the robot during a given period, and it is expressed as

$$displacement = \sqrt{(x(N) - x(0))^2 + (y(N) - y(0))^2 + (z(N) - z(0))^2}, \quad (\text{S.16})$$

where x , y , and z denote distances along three directions in world coordinate, and N indicates the total sample size.

7. Parameter setup of the adaptive quadruped motor control

The instructions of how to setup the parameters of the DFFB reflex, CPGs, MNs, and DIL are described as below (see also Table S.3):

1. **DFFB reflex:** The DFFB reflex has four parameters: $w_1(n)$, $w_2(n)$, w_3 and w_4 . They are configured as:
 - i) The two adaptive synaptic weights $w_1(n)$ and $w_2(n)$ are positive. They determine the sensory gain of the DFFB reflex. According to our experience and empirically study, their proper initial values should be small, i.e. 0.003 and 0.0032, respectively. However, when the DIL is induced to adjust the two parameter values online (i.e., adaptive sensory gain), their initial values can also be simply set to zero without specific initialization. In conclusion, the initialization for the two values is only necessary for employing the DFFB reflex when the DIL is not applied, i.e., fixed sensory gain. A further analysis of the adaptive or fixed sensory feedback gain can also be seen in [9].
 - ii) The two constant parameters w_3 and w_4 are the output gains of the DFFB reflex to the knee and hip joints, respectively. They are set to fixed values 2.0 and 1.0, respectively. This is because the foot displacement controlled by the hip joint will be approximately twice of that controlled by the knee joint if the two joints receive the same command values. Therefore, we compensate for this by setting the w_3 value controlling the knee joint to twice the w_4 value controlling the hip joint.
2. **CPGs:** Each CPG is based on the special orthogonal group (SO(2)) CPG proposed in [10]. Here, four CPGs are used and coupled. They have four constant parameters: \mathbf{w} , \mathbf{b} , Φ , and ϵ which are configured as follows:
 - i) \mathbf{w} and \mathbf{b} are synaptic weights and biases of the four CPGs. \mathbf{w} determines the shape and frequency of the CPG outputs. \mathbf{b} is for activating the neurons of the CPGs. Its value can be initialized in a range of (-0.085, 0.085). Based on the background of well understood the neurodynamics of the SO(2) CPG [10], the weight parameters were manually selected (see Table S.3) in accordance with staying near the Neimark-Sacker bifurcation set where quasi-periodic attractors occur. The attractors can drive the joints to perform rhythmic movements. The detailed dynamical analysis and parameter setting of the SO(2) CPGs can be see in [10].
 - ii) Φ and ϵ represent relative phases and coupling strength among the four CPGs. For instance, ϕ_{12} and ϕ_{13} represent the relative phases of the second CPG (controlling right hind leg) and the third CPG (controlling the left front leg) with respect to the first CPG (controlling the right front leg). Here, we used a trot gait for all robot experiments, where the diagonal legs move in-phase but anti-phase with other legs. Therefore, the CPGs of the right hind and left front legs are in-phase but out-of-phase with the CPG of the right front leg. Accordingly, $\phi_{23} = 0$, ϕ_{12} and ϕ_{13} equal to $-\pi$. ϵ determines the CPG coupling strength, i.e., the larger of this value, the stronger the CPG relative phase locking. For this parameter setup, we empirically increased its value from zero to the value that the CPGs can show proper phase relationship for the trot gait. This CPG phase locking technique was proposed by Shinya et. al. [11].
3. **MNs:** The MNs is for integrating the signals from the CPGs and the DFFB reflex and linearly scaling the integrated signals to expected joint movement positions [12, 13]. The MNs have two parameters: α and $\beta(n)$ which are configured as follows:
 - i) α determines the amplitudes of the joint movement commands corresponding to the leg step height and length. This parameter can properly match the commands to the robot joint movement work space. In the experiments, we empirically set the parameter to 0.16 for Lilibot and 0.12 for Laikago according to the robots' configurations.
 - ii) $\beta(n)$ determines the joint movement offsets. It influences the robot walking posture. This parameter was initially set to zero and further modulated online by the DFFB reflex.
4. **DIL:** The DIL has six parameters: A_f , B_f , and C_f for fast learner, as well as A_s , B_s , and C_s for slow learner. A_f and A_s are the retention factors, B_f and B_s are the learning rates, and C_f and C_s are the integral rates. The parameter selection is under the constraint that $B_f > B_s$, $A_f < A_s$, and $C_f > C_s$. The DIL does not require its parameters to be precisely set to fit specific situations. Thus, here we set these parameters (see Table S.3) based on previous studies [14, 15].

Table S.3: Parameters of the adaptive quadruped motor control (AQMC).

Modules	Symbols	Initial values	Description	Adaptive /constant
CPGs [10, 11]	\mathbf{w}	$\begin{pmatrix} 1.4 & 2.6 \\ -2.6 & 1.4 \end{pmatrix}$	Synaptic weights of the SO(2) CPG neurons (see Eq. (1) in the main manuscript)	Constant
	\mathbf{b}	$\begin{pmatrix} 0.01 & 0.01 & 0.01 & 0.01 \\ 0.01 & 0.01 & 0.01 & 0.01 \end{pmatrix}$	Biases of the SO(2) CPG neurons for triggering CPG activation (see Eq. (1) in the main manuscript)	Constant
	Φ	$\begin{pmatrix} 0.0 & -\pi & -\pi & 0.0 \\ \pi & 0.0 & 0.0 & \pi \\ \pi & 0.0 & 0.0 & \pi \\ 0.0 & -\pi & -\pi & 0.0 \end{pmatrix}$	Desired relative phases among the four CPGs (see Eqs. (3) and (4) in the main manuscript)	Constant
	ϵ	0.01	CPG communication gain (see Eq. (3) in the main manuscript)	Constant
MNs [12, 13]	α	0.16 for Lilibot and 0.12 for Laikago	Synaptic weight projection from the CPGs to MNs (see Eq. (5) in the main manuscript)	Constant
	$\beta_{1,2}(n)$	0	Online modulated by the DFFB (see Eqs. (5) and (10) in the main manuscript)	Adaptive
DFFB reflex	$w_1(n)$	0.003	Online modulated by the DIL (see Eq. (12) in the main manuscript)	Adaptive
	$w_2(n)$	0.0032	Online modulated by the DIL (see Eq. (12) in the main manuscript)	Adaptive
	w_3	2	DFFB output gain of the knee joint (see Fig. 5 in the main manuscript)	Constant
	w_4	1	DFFB output gain of the hip joint (see Fig. 5 in the main manuscript)	Constant
DIL [14, 15]	A_f	0.01	Retention rate of the fast learner (see Eq. (11) in the main manuscript)	Constant
	B_f	0.05	Learning rate of the fast learner (see Eq. (11) in the main manuscript)	Constant
	C_f	0.001	Integral rate of the fast learner (see Eq. (11) in the main manuscript)	Constant
	A_s	0.1	Retention rate of the slow learner (see Eq. (11) in the main manuscript)	Constant
	B_s	0.01	Learning rate of the slow learner (see Eq. (11) in the main manuscript)	Constant
	C_s	0.0001	Integral rate of the slow learner (see Eq. (11) in the main manuscript)	Constant

References

- [1] J. Nakanishi, J. Morimoto, G. Endo, G. Cheng, S. Schaal, M. Kawato, A framework for learning biped locomotion with dynamical movement primitives, in: 4th IEEE/RAS International Conference on Humanoid Robots, 2004., Vol. 2, IEEE, 2004, pp. 925–940. doi:10.1109/ICHR.2004.1442695.
- [2] A. J. Ijspeert, J. Nakanishi, H. Hoffmann, P. Pastor, S. Schaal, Dynamical movement primitives: learning attractor models for motor behaviors, *Neural Computation* 25 (2) (2013) 328–373. doi:10.1162/NECO_a_00393.
- [3] S. Schaal, C. G. Atkeson, Constructive incremental learning from only local information, *Neural Computation* 10 (8) (1998) 2047–2084.
- [4] J. Nakanishi, J. Morimoto, G. Endo, G. Cheng, S. Schaal, M. Kawato, Learning from demonstration and adaptation of biped locomotion with dynamical movement primitives, in: Workshop on Robot Programming by Demonstration, IEEE/RSJ International Conference on Intelligent Robots and Systems, 2003.
- [5] M. Focchi, A. Del Prete, I. Havoutis, R. Featherstone, D. G. Caldwell, C. Semini, High-slope terrain locomotion for torque-controlled quadruped robots, *Autonomous Robots* 41 (1) (2017) 259–272.
- [6] T. Sun, X. Xiong, Z. Dai, P. Manoonpong, Small-sized reconfigurable quadruped robot with multiple sensory feedback for studying adaptive and versatile behaviors, *Frontiers in Neurorobotics* 14 (2020) 14. doi:10.3389/fnbot.2020.00014.
- [7] M. Iosa, T. Marro, S. Paolucci, D. Morelli, Stability and harmony of gait in children with cerebral palsy, *Research in Developmental Disabilities* 33 (1) (2012) 129–135.
- [8] C. Ferreira, C. P. Santos, A sensory-driven controller for quadruped locomotion, *Biological Cybernetics* 111 (1) (2017) 49–67.
- [9] A. Miguel-Blanco, P. Manoonpong, General distributed neural control and sensory adaptation for self-organized locomotion and fast adaptation to damage of walking robots, *Frontiers in Neural Circuits* 14 (2020) 46. doi:doi:10.3389/fncir.2020.00046.
- [10] F. Pasemann, M. Hild, K. Zahedi, So(2)-networks as neural oscillators, in: Computational Methods in Neural Modeling, Springer Berlin Heidelberg, Berlin, Heidelberg, 2003, pp. 144–151. doi:10.1007/3-540-44868-3_19.
- [11] S. Aoi, T. Yamashita, K. Tsuchiya, Hysteresis in the gait transition of a quadruped investigated using simple body mechanical and oscillator network models, *Physical Review E* 83 (6) (2011) 061909. doi:10.1103/PhysRevE.83.061909.
- [12] T. Sun, D. Shao, Z. Dai, P. Manoonpong, Adaptive neural control for self-organized locomotion and obstacle negotiation of quadruped robots, in: 2018 27th IEEE International Symposium on Robot and Human Interactive Communication (RO-MAN), IEEE, 2018, pp. 1081–1086. doi:10.1109/ROMAN.2018.8525645.
- [13] T. Sun, X. Xiong, Z. Dai, D. Owaki, P. Manoonpong, A comparative study of adaptive interlimb coordination mechanisms for self-organized robot locomotion, *Frontiers in Robotics and AI* 8 (2021) 86. doi:10.3389/frobt.2021.638684.
- [14] M. Thor, P. Manoonpong, Error-based learning mechanism for fast online adaptation in robot motor control, *IEEE Transactions on Neural Networks and Learning Systems* 31 (6) (2020) 2042–2051. doi:10.1109/TNNLS.2019.2927737.
- [15] M. A. Smith, A. Ghazizadeh, R. Shadmehr, Interacting adaptive processes with different timescales underlie short-term motor learning, *PLoS Biol* 4 (6) (2006) e179. doi:10.1371/journal.pbio.0040179.